

Building and characterizing a stylus ion-trap system

Tai-Hao Cui(崔太豪), Ya-Qi Wei(魏雅琪), Ji Li(李冀), Quan Yuan(袁泉), Shuang-Qing Dai(戴双晴), Pei-Dong Li(李沛东), Fei Zhou(周飞), Jian-Qi Zhang(张建奇), Zhu-Jun Zheng(郑驻军), Liang Chen(陈亮), and Mang Feng(冯芒)

Citation: Chin. Phys. B, 2024, 33 (**4**): 043701. DOI: 10.1088/1674-1056/ad22d9
Journal homepage: http://cpb.iphy.ac.cn; http://iopscience.iop.org/cpb

What follows is a list of articles you may be interested in

High efficient Raman sideband cooling and strong three-body recombination of atoms

Yuqing Li(李玉清), Zhennan Liu(刘震南), Yunfei Wang(王云飞), Jizhou Wu(武寄洲), Wenliang Liu(刘文良), Yongming Fu(付永明), Peng Li(李鹏), Jie Ma(马杰), Liantuan Xiao(肖连团), and Suotang Jia(贾锁堂)

Chin. Phys. B, 2023, 32 (**10**): 103701. DOI: 10.1088/1674-1056/acec42

Quantum degenerate Bose-Fermi atomic gas mixture of ^{23}Na and ^{40}K

Ziliang Li(李子亮), Zhengyu Gu(顾正宇), Zhenlian Shi(师振莲), Pengjun Wang(王鹏军), and Jing Zhang(张靖)

Chin. Phys. B, 2023, 32 (**2**): 023701. DOI: 10.1088/1674-1056/aca14f

Space continuous atom laser in one dimension

Yi Qin(秦毅), Xiao-Yang Shen(沈晓阳), Wei-Xuan Chang(常炜玄), and Lin Xia(夏林)

Chin. Phys. B, 2023, 32 (**1**): 013701. DOI: 10.1088/1674-1056/ac7861

Superfluid to Mott-insulator transition in a one-dimensional optical lattice

Wenliang Liu(刘文良), Ningxuan Zheng(郑宁宣), Jun Jian(蹇君), Li Tian(田丽), Jizhou Wu(武寄洲), Yuqing Li(李玉清), Yongming Fu(付永明), Peng Li(李鹏), Vladimir Sovkov, Jie Ma(马杰), Liantuan Xiao(肖连团), and Suotang Jia(贾锁堂)

Chin. Phys. B, 2022, 31 (**7**): 073702. DOI: 10.1088/1674-1056/ac6579

Enhanced cold mercury atom production with two-dimensional magneto-optical trap

Ye Zhang(张晔), Qi-Xin Liu(刘琪鑫), Jian-Fang Sun(孙剑芳), Zhen Xu(徐震), and Yu-Zhu Wang(王育竹)

Chin. Phys. B, 2022, 31 (**7**): 073701. DOI: 10.1088/1674-1056/ac5397

INSTRUMENTATION AND MEASUREMENT

Building and characterizing a stylus ion-trap system

Tai-Hao Cui(崔太豪)[1,2,†], Ya-Qi Wei(魏雅琪)[3,†], Ji Li(李冀)[4,†], Quan Yuan(袁泉)[1], Shuang-Qing Dai(戴双晴)[1,2], Pei-Dong Li(李沛东)[1,2], Fei Zhou(周飞)[1,4], Jian-Qi Zhang(张建奇)[1], Zhu-Jun Zheng(郑驻军)[3,†], Liang Chen(陈亮)[1,4,‡], and Mang Feng(冯芒)[1,4,5,§]

[1] *State Key Laboratory of Magnetic Resonance and Atomic and Molecular Physics, Wuhan Institute of Physics and Mathematics, Innovation Academy of Precision Measurement Science and Technology, Chinese Academy of Sciences, Wuhan* 430071, *China*

[2] *University of the Chinese Academy of Sciences, Beijing* 100049, *China*

[3] *Laboratory of Quantum Science and Engineering, South China University of Technology, Guangzhou* 510641, *China*

[4] *Research Center for Quantum Precision Measurement, Guangzhou Institute of Industry Technology, Guangzhou* 511458, *China*

[5] *Department of Physics, Zhejiang Normal University, Jinhua* 321004, *China*

(Received 24 December 2023; revised manuscript received 13 January 2024; accepted manuscript online 26 January 2024)

Cold trapped ions can be excellent sensors for ultra-precision detection of physical quantities, which strongly depends on the measurement situation at hand. The stylus ion trap, formed by two concentric cylinders over a ground plane, holds the promise of relatively simple structure and larger solid angle for optical access and fluorescence collection in comparison with the conventional ion traps. Here we report our fabrication and characterization of the first stylus ion trap constructed in China, aiming for studying quantum optics and sensing weak electric fields in the future. We have observed the stable confinement of the ion in the trapping potential for more than two hours and measured the heating rate of the trap to be $\mathrm{d}\varepsilon/\mathrm{d}t = 7.10 \pm 0.13$ meV/s by the Doppler recooling method. Our work starts a way to building practical quantum sensors with high efficiency of optical collection and with ultimate goal for contributing to future quantum information technology.

Keywords: stylus ion trap, electric-field noises, Doppler recooling method, heating rate

PACS: 37.10.De, 07.07.Df, 07.77.Ka **DOI:** 10.1088/1674-1056/ad22d9

1. Introduction

Atomic sensors developed over the past years have attracted much attention due to their higher sensitivity than ever before in the detection of various physical quantities.[1] Besides, they also own the superiority of high resolution, fast response and broad range of adjustibility, which are very helpful in practical application.

In the present work, we report our fabrication and characterization of a stylus ion trap, which aims to detect electric field noises.[2–5] Trapped ultracold ions with high-precision manipulation are an ideal platform for precision measurement.[6,7] In particular, the strong coupling to external electric fields makes the trapped ions excellent sensors for characterizing weak variation of the external electric fields.[8–10] In ion traps, the electric field fluctuations are typical types of noises, leading to instability of the trapped ions, *i.e.*, the main detrimental factor for confining and manipulating the ions.[11,12] Generally speaking, electric-field noises above surfaces provide a significant challenge to many disparate areas of physics, from instability of the system to imprecision of measurement.[13] We have noticed recent efforts exploring the detection of noise spectra using harmonic oscillators.[14–16] The basic ideas in these works are enacted on the laser-cooled trapped ions prepared in vibrational ground state and varied with resonance frequencies. With these single-ion sensors, the intrinsic noise spectra of the ion-trap potentials were experimentally identified and demonstrated. The electric-field noise leads to the motional heating. In addition, the electric-field noise stemming from the adsorption surface is found to be the main reason for the fluctuation of the secular frequency and thus decoherence in the ion trap.[17,18] In this context, the single-ion sensors can work for noise detection in a wide variety of experiments, going beyond the problems of the ion traps themselves, to offer new ways for, *e.g.*, probing the electric-field noise of proximate surfaces of interest. This helps analyzing surfaces to complement the existing surface-science toolbox.

Optimization of the sensing technique of the trapped ions depends on higher fluorescence collection efficiency and better stability conditions. The stylus ion trap introduced here is a specialized trap with enhanced solid angle access to the trapped ion, see schematic comparison in Fig. 1, where the external surfaces of interest are brought into close proximity to the single-ion sensors confined in different ion traps. The changes of the heating rates of the single-ion sensors are measured to determine the electric-field noises added by the exter-

[†]These authors contributed equally to this work.

[‡]Corresponding author. E-mail: liangchen@wipm.ac.cn

[§]Corresponding author. E-mail: mangfeng@wipm.ac.cn

© 2024 Chinese Physical Society and IOP Publishing Ltd

nal sample's surfaces. The ion confined in the stylus trap, with larger solid angle for the fluorescence collection, can detect the surface noise with higher efficiency than the counterparts in usual surface electrode traps.[19] When we assume the distance $h = 330$ μm and $d = 300$ μm, we find numerically that the solid angle ϕ_2 is 4 times larger than the solid angle ϕ_4.

As the prerequisite of the noise detection as plotted in Fig. 1(a), the first stylus ion trap system has been constructed in China (see Fig. 2). In what follows, we introduce the structure of this trap and characterize its performance, including the stable confinement of the ion and the heating rate of the trap. After the optimization, we have observed the stable confinement of the single ion in the stylus trap for more than two hours.

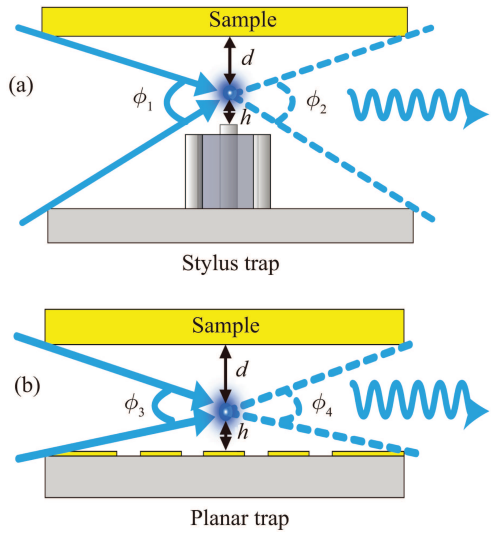


Fig. 1. Comparisons of different ion traps for sensing the electric-field noises of the proximate surfaces of interest, where the trapped ions are located above the nearest electrodes by the same distance h, and the surfaces to be detected are moved into close proximity to the ions by the same distance d. (a) The stylus trap with the solid angles ϕ_1 and ϕ_2 for optical access and fluorescence collection, respectively. (b) The planar trap with the solid angles ϕ_3 and ϕ_4 for optical access and fluorescence collection, respectively. The solid (dashed) arrows represent the input laser beams (the fluorescence emission).

2. Characterization of the trap

As shown in Fig. 2, we have fabricated a stylus ion trap, and successfully confined a single $^{40}Ca^{+}$ ion with the height of $h \simeq 330$ μm above the central electrode. The trap consists of two concentric cylinders and four cylindrical dc electrodes (see Fig. 2(b)). The two concentric cylinders include a hollow-cylinder rf electrode and a central dc electrode, the former of which provides the radio-frequency (rf) confinement of the ion. The four cylindrical dc electrodes, with each of the diameter of 400 μm, are distributed equidistantly outside the concentric cylinders, compensating the stray electric fields. The rf electrode owns an inner diameter of 0.8 mm and an outer diameter of 1.4 mm. The central electrode is of the diameter of 400 μm. The dc and rf electrodes are 1.8-mm high, and the central electrode takes a height of 2.05 mm.

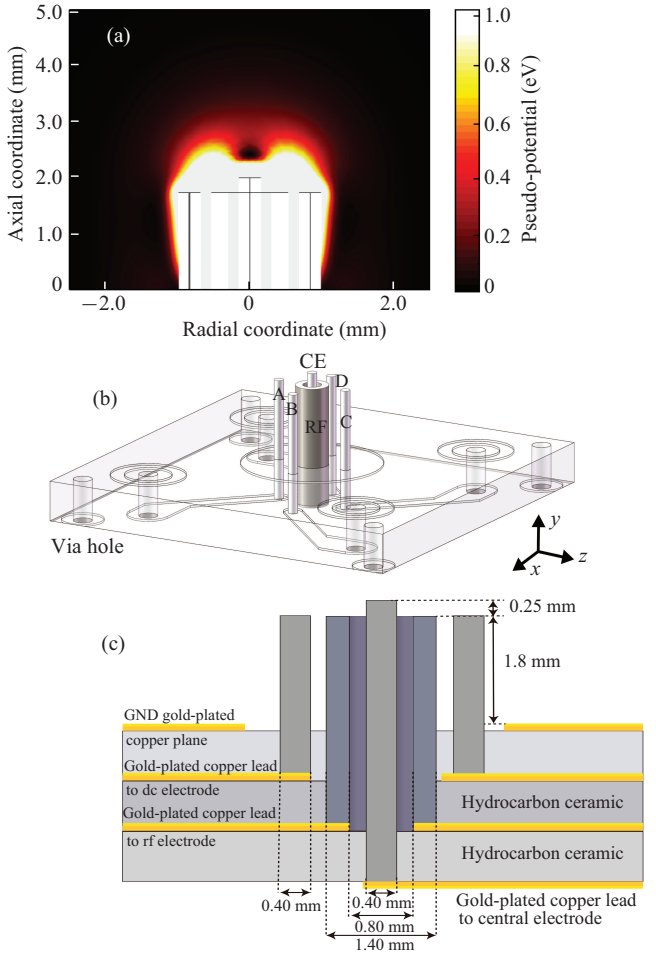


Fig. 2. The pseudo-potential and trap geometry of the stylus ion trap. (a) Simulation of the trap pseudo-potential. (b) Placement of the electrodes, where CE is the central electrode, RF is the rf electrode, and A, B, C, and D represent the four dc electrodes. The via hole is to connect to circuits at different layers. (c) The profile map of the trap showing the layered assemble and the conducting gold leads.

We apply a voltage $V_{\rm rf}\cos(\Omega_{\rm rf}t)$ on the rf electrode and connect other electrodes to the ground. The rf pseudo-potential could be described by the solution of the Laplace equation[20]

$$\Phi(x,y,z) = \frac{QV_{\rm rf}^2}{4m\Omega_{\rm rf}^2} \mid \nabla\phi_{\rm rf}(x,y,z) \mid^2, \tag{1}$$

where m is the mass of the ion, $\Omega_{\rm rf}$ is the rf frequency, Q is the charge of the ion, and $\phi_{\rm rf}(x,y,z)$ is the rf potential basis function. We simulate the potential of the stylus ion trap by a commercial software (COMSOL Multiphysics5.5), as shown in Fig. 2(a). In our simulation, we set $V_{\rm rf} = 350$ V and $\Omega_{\rm rf}/2\pi = 13.78$ MHz. Compared with the conventional ion traps (*e.g.*, the linear traps and the surface-electrode traps) under the same conditions, the stylus trap owns a shallower potential well with the depth of only 0.45 eV. The electrodes are made of the custom-made chrome-nickel-molybdenum alloy steel with superior strength and high temperature resistance. The bottom layer of the stylus trap is composed of three layers of plates, as plotted in Fig. 2(c). The base plates, made of Rogers hydrocarbon ceramics (Rogers4350B) to ensure good

insulation between different plates, are processed by printed circuit board technology with electrical connection holes such as vias reserved. The gold layer is deposited on the copper surface to prevent the electrodes from oxidating. The thickness of the copper layer is about 35 μm, and the thickness of the plate under the copper layer is about 0.88 mm. The electrodes and copper layer are connected by tin soldering through the preset electrical via holes.

Figure 3(a) sketches the experimental system of the stylus trap, in which the stylus trap is installed into the steel vacuum chamber (not shown). The vacuum is maintained by the ion pumper and the non-evapotranspiration Getter pumper, making the actual pressure lower than 10^{-10} mbar inside the chamber. Figure 3(b) demonstrates the picture of the completed stylus trap. The rf electrode connects to a home-made helical resonator which owns the quality factor of 200 and to an amplifier (LZY-22+, Mini-circuit). Then the rf electrode and the helical resonator form a resonant LC circuit with the resonance frequency $\Omega_{\rm rf}/2\pi = 13.78$ MHz and the rf peak-to-peak voltage 350 V. Under the pseudo-potential assumption, the trap works with the three-dimensional frequencies $\omega_y/2\pi = 1516.5$ kHz, $\omega_z/2\pi = 761.0$ kHz, and $\omega_x/2\pi = 770.0$ kHz.

The dc voltages applied to the central electrode and the four dc electrodes vary from -10.0 V to 10.0 V, which are provided by an analog output card (PCI-6733, National Instruments). We employ the dc voltages to control and minimize the unwanted micromotion of the ion for suppressing the Doppler shifts and improving the cooling efficiency. To minimize the micromotion of the ion, we first carefully adjust the dc voltages until the ion is moved to a position insensitive to the rf drive.[21] Then, the rf frequency modulation and the rf-photon correlation technology are employed to further reduce the micromotion of the ion.[22,23]

3. Measurement of heating rate

Now we show the measurement of the heating rate of the stylus trap. The heating rate of the ion trap is an important metric for evaluating its performance relevant to the temperature and the decoherence time of the trapped ion[24] as well as the measurement precision in the experiments.[11] There are two commonly employed approaches to acquire the heating rate of the ion trap. The most recognized approach is based on the sideband absorption spectrum,[25,26] which requires the ion to be cooled down to near the motional ground state of the trap. Thus it is employed along with the sub-Doppler cooling schemes, such as the sideband cooling,[27] the electromagnetically induced transparency cooling[28] and the polarization gradient cooling.[29] Another approach is the Doppler recooling method in which the motional energy of the ion is determined by taking advantage of the increased Doppler shift for an ion with increased kinetic energy. It is required to record the time-resolved fluorescence after the ions are heated up,[26,30] and estimate the ion's energy by comparing the instantaneous ion fluorescence to the steady-state fluorescence level of a Doppler-cooled ion. This method is more practical for evaluating the performance of new trapping systems. In our case, as clarified below, when the repumping laser beam at 866 nm is turned off for a while, we estimate the heating rate of the trapped ion by detecting the energy change of the ion with respect to the heating time (*i.e.*, the off time of the 866-nm laser).

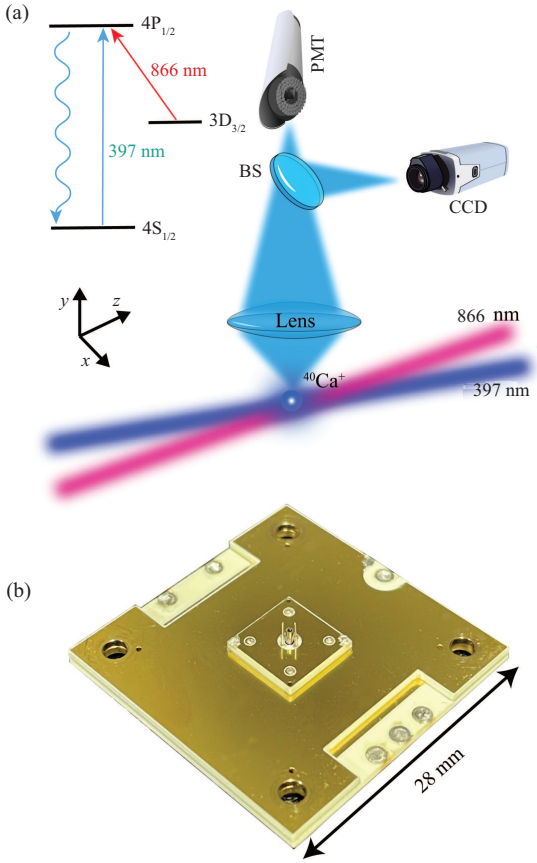


Fig. 3. Schematic diagram of the stylus ion trap system. (a) Measurement of the heating rate. PMT: the photomultiplier tube for recording the emitting fluorescence from the trapped ion. CCD: the charge-coupled device camera for taking images of the ion. The spontaneous emission fluorescence of the ion is first collected by the lens, which is 1.70% of the total emission. The ratio of the beam splitter (BS) is 7/3 for the PMT to the CCD. Two lasers with wavelengths of 397 nm and 866 nm, respectively, are employed for cooling the ion. Other two laser beams at 423 nm and 375 nm, employed for photon-ionization, are not shown here for simplicity. (b) Photograph of the completed stylus trap. The trap is of the form of square with each side being 28 mm.

To perform the Doppler recooling method, we should first cool the trapped ion to its Doppler cooling limit, and then we turn off the Doppler cooling by shutting down the 866 nm repumping laser for a period $\tau_{\rm off}$, during which the ion is heated up. The fluorescence change of the ion is monitored as the ion is cooled down again after the Doppler cooling restarts. This fluorescence change can be considered as the energy gain of the ion during the off time of $\tau_{\rm off}$ and thus we can deduce the heating rate of the ion. During this process, the micromotion

of the ion is the main factor to cause the fluorescence fluctuation and the Doppler broadening. Moreover, using the Doppler recooling method to estimate the ion's energy requires exact knowledge of the linewidth of the resonance and the saturation parameters. For the multi-level dynamics in our case, the detailed modeling of the dynamics and careful measurement of all relevant laser parameters, such as detunings and intensities, are necessary, which is too complicated to accomplish. As a result, we will employ a workaround, following the idea from Ref. [31], by calibrating the energy scale with externally applied electric field noises. By fitting the fluorescence data as a function of time, we acquire curves of the mean energy of the ion. By fitting the fluorescence data as a function of the noise intensity, we acquire the change rate of the mean energy, *i.e.*, the heating rates.

The external electric-field noises, generated from the signal generator, are applied on the central electrode to accelerate the energy variation of the ion in our measurement of heating rates. We choose the type of the noise as the zero-mean Gaussian white noise, which takes the peak voltage from 8 mV to 12 mV. The noises are weak, not affecting the stable confinement of the ion, while bringing in additional heating. The fluorescence data are recorded by the multi-channel scaler (SR430), which, to avoid any data loss, is switched on when the ion is still heating (*e.g.*, for $\tau_{\rm u}$ before the fluorescence is restored). The multi-channel scaler can possess 1024 channels, where the time bin of each channel is set to be 162 μs. Each measurement has accumulated the data by 100 times and repeated this measurement by five times.

After removing the invalid data recorded during the period $\tau_{\rm u}$, we obtain the Doppler recooling curves, as shown in Fig. 4. We can acquire the energy of the ion from the curves by the method proposed in Ref. [30]. The red solid curve is fitted based on the following thermally averaged scattering rate:

$$\left\langle \frac{\mathrm{d}N}{\mathrm{d}\tau} \right\rangle_{\bar{\varepsilon}} = \int_0^{\infty} P_0(\varepsilon') \left. \frac{\mathrm{d}N}{\mathrm{d}\tau} \right|_{\varepsilon=\Xi(\varepsilon',\tau)} \mathrm{d}\varepsilon', \tag{2}$$

with the initial energy $\varepsilon(\tau=0)=\varepsilon'$ and the energy $\Xi(\varepsilon',\tau)$ at time τ of the ion, as well as the mean energy $\bar{\varepsilon}$. In Eq. (2), $P_0(\varepsilon)=\mathrm{e}^{-\varepsilon/\bar{\varepsilon}}/\bar{\varepsilon}$ represents the Maxwell–Boltzmann distribution of the motional energies at the beginning of each cooling period. $\mathrm{d}N/\mathrm{d}\tau=\mathrm{Im}(Z)/\sqrt{4\varepsilon r}$ is the scattering rate with $Z=\mathrm{i}/\sqrt{1-(\delta+\mathrm{i})^2/4\varepsilon\delta}$. The energy ε can be inferred by $\mathrm{d}\varepsilon/\mathrm{d}\tau=[\mathrm{Re}(Z)+\delta\mathrm{Im}(Z)]/\sqrt{4\varepsilon r}$ with the initial energy ε' and $\delta=2\Delta/\Gamma\sqrt{1+s}$. The parameter values in our experiment are given by $\Delta/2\pi=-10$ MHz, $\Gamma/2\pi=21$ MHz, $r=0.0019$ and $s=1.5$.

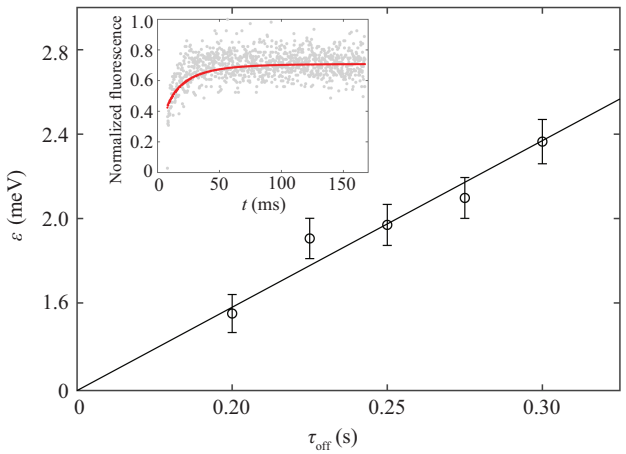


Fig. 4. Scaled energy ε as a function of the heating time $\tau_{\rm off}$ in the Doppler recooling experiment. The heating time $\tau_{\rm off}$ varies from 200 ms to 300 ms with the time interval of 25 ms. The external electric-field noise is applied with the intensity fixed at 9 mV. The energy of the ion increases linearly with $\tau_{\rm off}$, and the heating rate $\mathrm{d}\varepsilon/\mathrm{d}t=7.89\pm0.048$ meV/s is acquired by linearly fitting the experimental values. Inset: the fluorescence versus $\tau_{\rm off}$, and the corresponding time bin is 162 μs. The 397-nm laser with the intensity of 0.318 W/cm^2 and the detuning of -10 MHz, couples $S_{1/2}$ to $P_{1/2}$ for Doppler cooling and fluorescence detection. The 866-nm laser takes the intensity of 0.547 W/cm^2, driving resonantly the transition between $P_{1/2}$ and $D_{3/2}$.

Figure 5 plots the heating rates of the stylus trap as functions of the externally applied noises with different intensities, in which each point corresponds to a line measured in Fig. 4. Due to the complicated noisy situation in the stylus trap, our measurement is time-consuming, leading to a minimum separation of 10 hours in the measurement of the different curves in Fig. 5. Based on these observations, we estimate, by the linear fitting, the average heating rate of the stylus trap to be $\mathrm{d}\varepsilon/\mathrm{d}t=7.10\pm0.13$ meV/s in the absence of the external noises.

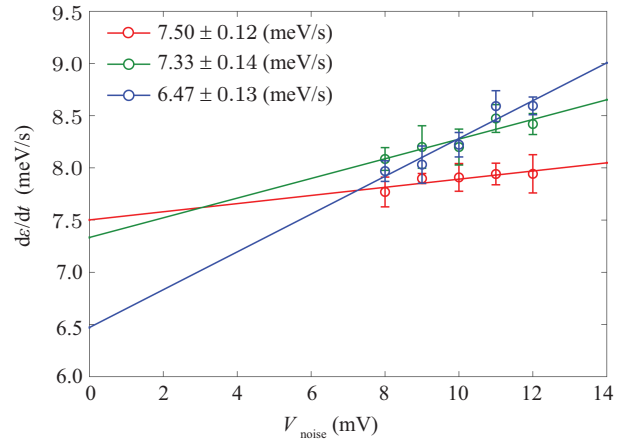


Fig. 5. The heating rate *versus* the the peak voltage of externally applied noises. Here the complexity of the noises in the trap system are reflected in the large difference among the curves acquired experimentally. The heating rate of the stylus trap is the average of the values of the three curves at $V_{\rm noise}=0$ mV.

4. Discussion and conclusion

As mentioned in Section 1, the straightforward application of the stylus trap is for practically and precisely detecting

heating rates of different surfaces of interest moved in close proximity to the ion sensor. To this end, suppressing the background noises and the detection uncertainty relevant to the ion sensor is essential to the measurement precision in the practical application. Due to the special geometry of the stylus ion trap, however, the rf electrode in the concentric cylinders, which is distant from the the location of the trapped ion by 330 μm, provides a serious heating to the ion. Also due to the special geometry, we are unable to perform the laser cooling along the y direction. Thus the micromotion compensation could not be well accomplished, which leads to relatively higher heating rates than the linear traps. As such, further efforts need to be paid on compensating the micromotion. Moreover, from the observation in Figs. 4 and 5, we consider that the statistical errors originate from the frequency and power instability of the lasers as well as the unexpected position drift of the ion. Therefore, further improving the stability of optical and electrical setups is highly expected.

We have also found that part of the heating effect comes from the unexpected calcium powder adhered to the electrode surface of the trap. To suppress this detrimental effect, we will adopt the method of laser ablation[32,33] in the future, instead of the currently used electron bombardment method, in the generation of the neutral calcium atoms. In addition, we will also consider the assistance from the helium bath cryostat, which can effectively reduce the ambient temperature and the heating rate.[34] Moreover, we will fabricate the stylus ion trap using non-magnetic metal, such as the titanium, to reduce the unexpected magnetic effect, and we will also enhance the conduction of the electrodes through the gold-plating process.[35] Furthermore, cleaning the surface of the trap is helpful for remaining the low-noise level in the ion-trap system. We will carry out the surface cleaning[36] for the stylus trap using high-power lasers. It is anticipated for our next work that we could reduce the heating rate of the stylus trap by two orders of magnitudes, corresponding to the electric-field-noise spectral density of $10^{-12}\ \mathrm{V}^2\cdot\mathrm{m}^{-2}\cdot\mathrm{Hz}^{-1}$. At this level, we are hopefully able to distinguish different electric-field noises of the surface due to different blocks of metals, while still unable to distinguish the impurity atoms in adsorption if the noise originates from the surface adsorption of atoms. Exactly probing the latter noise requires the capability of the electric-field-noise detection to the level lower than $10^{-13}\ \mathrm{V}^2\cdot\mathrm{m}^{-2}\cdot\mathrm{Hz}^{-1}$.[37]

In summary, we have constructed and characterized a stylus ion trap and stably confined the ions in the trap. The performance of the trap system has been evaluated using the Doppler recooling method. To our knowledge, this is the first work in China to explore the stylus ion trap, which lays a solid foundation for practical trapped-ion sensors in the future. Further suppressing the noise in the trap system is necessary for developing the new platform as an ultra-precision sensor system. The present results start the way to understanding the working mechanism of the real stylus trap potential, which would be helpful for developing a brand-new surface-science tool for studying anomalous heating[18,36,38,39] and materials science.[40–42]

Acknowledgments

Project supported by the Special Project for Research and Development in Key Areas of Guangdong Province, China (Grant No. 2020B0303300001), the National Natural Science Foundation of China (Grant Nos. U21A20434, 12074346, 12074390, 11835011, 11804375, and 11804308), the Fund from the Key Laboratory of Guangzhou for Quantum Precision Measurement (Grant No. 202201000010), the Science and Technology Projects in Guangzhou (Grant No. 202201011727), and the Nansha Senior Leading Talent Team Technology Project (Grant No. 2021CXTD02).

References

[1] Degen C L, Reinhard F and Cappellaro P 2017 *Rev. Mod. Phys.* **89** 035002
[2] Maiwald R, Leibfried D, Britton J, Bergquist J C, Leuchs G and Wineland D J 2009 *Nat. Phys.* **5** 551
[3] Arrington C L, McKay K S, Baca E D, Coleman J J, Colombe Y, Finnegan P, Hite D A, Hollowell A E, Jördens R, Jost J D, Leibfried D, Rowen A M, Warring U, Weides M, Wilson A C, Wineland D J and Pappas D P 2013 *Rev. Sci. Instrum.* **84** 085001
[4] Hite D A, McKay K S, Kotler S, Leibfried D, Wineland D J and Pappas D P 2017 *MRS Adv.* **2** 2189
[5] McKay K S, Hite D A, Kent P D, Kotler S, Leibfried D, Slichter D H, Wilson A C and Pappas D P 2021 *Phys. Rev. A.* **104** 052610
[6] Kotler S, Akerman N, Glickman Y, Keselman A and Ozeri R 2011 *Nature.* **473** 61
[7] Burd S C, Srinivas R, Bollinger J J, Wilson A C, Wineland D J, Leibfried D, Slichter D H and Allcock D T C 2019 *Science* **364** 1163
[8] Liu Z C, Wei Y Q, Chen L, Li J, Dai S Q, Zhou F and Feng M 2021 *Phys. Rev. Appl.* **16** 044007
[9] Wei Y Q, Wang Y Z, Liu Z C, Cui T H, Chen L, Li J, Dai S Q, Zhou F and Feng M 2022 *Science China-Phys. Mech. Astron.* **65** 110313
[10] Wei Y Q, Yuan Q, Chen L, Cui T H, Li J, Dai S Q, Zhou F and Feng M 2023 *Phys. Rev. Appl.* **19** 064062
[11] Brownnutt M, Kumph M, Rabl P and Blatt R 2015 *Rev. Mod. Phys.* **87** 1419
[12] Turchette Q A, Kielpinski, King B E, Leibfried D, Meekhof D M, Myatt C J, Rowe M A, Sackett C A, Wood C S, Itano W M, Monroe C and Wineland D J 2000 *Phys. Rev. A.* **61** 063418
[13] Boldin I A, Kraft A and Wunderlich C 2018 *Phys. Rev. Lett.* **120** 023201
[14] Goldwater D, Barker P F, Bassi A and Donadi S 2019 *Phys. Rev. Lett.* **123** 230801
[15] Milne A R, Hempel C, Li L, Edmunds C L, Slatyer H J, Ball H, Hush M R and Biercuk M J 2021 *Phys. Rev. Lett.* **126** 250506
[16] Keller J, Hou P-Y, McCormick K C, Cole D C, Erickson S D, Wu J J, Wilson A C and Leibfried D 2021 *Phys. Rev. Lett.* **126** 250507
[17] Hite D A, Colombe Y, Wilson A C, Brown K R, Warring U, Jördens R, Jost J D, McKay K S, Pappas D P, Leibfried D and Wineland D J 2012 *Phys. Rev. Lett.* **109** 103001
[18] Dubessy R, Coudreau T and Guidoni L 2009 *Phys. Rev. A.* **80** 031402
[19] Maiwald R, Golla A, Fischer M, Bader M, Heugel S, Chalopin B, Sondermann M and Leuchs G 2012 *Phys. Rev. A.* **86** 043431
[20] Pearson C E, Leibrandt D R, Bakr W S, Mallard W J, Brown K R and Chuang I L 2006 *Phys. Rev. A.* **73** 032307

[21] Narayanan S, Daniilidis N, Möller S A, Clark R, Ziesel F, Singer K, Schmidt-Kaler F and H?ffner H 2011 *J. Appl. Phys.* **110** 114909

[22] Berkeland D J, Miller J D, Bergquist J C, Itano W M and Wineland D J 1998 *J. Appl. Phys.* **83** 5025

[23] Li J, Chen L, Chen Y-H, Liu Z-C, Zhang H and Feng M 2020 *Chin. Phys. Lett.* **37** 053701

[24] Deslauriers L, Olmschenk S, Stick D, Hensinger W K, Sterk J and Monroe C 2006 *Phys. Rev. Lett.* **97** 103007

[25] Roos C, Zeiger T, Rohde H, Nägerl H C, Eschner J, Leibfried D, Schmidt-Kaler F and Blatt R 1999 *Phys. Rev. Lett.* **83** 4713

[26] Epstein R J, Seidelin S, Leibfried D, Wesenberg J H, Bollinger J J, Amini J M, Blakestad R B, Britton J, Home J P, Itano W M, Jost J D, Knill E, Langer C, Ozeri R, Shiga N and Wineland D J 2007 *Phys. Rev. A.* **76** 033411

[27] Monroe C, Meekhof D M, King B E, Jefferts S R, Itano W M, Wineland D J and Gould P 1995 *Phys. Rev. Lett.* **75** 4011

[28] Roos C F, Leibfried D, Mundt A, Schmidt-Kaler F, Eschner J and Blatt R 2000 *Phys. Rev. Lett.* **85** 5547

[29] Ejtemaee S and Haljan P C 2017 *Phys. Rev. Lett.* **119** 043001

[30] Wesenberg J H, Epstein R J, Leibfried D, Blakestad R B, Britton J, Home J P, Itano W M, Jost J D, Knill E, Langer C, Ozeri R, Seidelin S and Wineland D J 2007 *Phys. Rev. A* **76** 053416

[31] Daniilidis N, Narayanan S, Möller S A, Clark R, Lee T E, Leek P J, Wallraff A, Schulz S, Schmidt-Kaler F and Häffner H 2012 *New J. Phys.* **14** 079504

[32] Kjaergaard N, Hornekaer L, Thommesen A M, Videsen Z and Drewsen M 2000 *Appl. Phys. B* **71** 207

[33] Gulde S, Rotter D, Barton P, Schmidt-Kaler F, Blatt R and Hogervorst W 2001 *Appl. Phys. B* **73** 861

[34] Labaziewicz J, Ge Y, Leibrandt D R, Wang S X, Shewmon R and Chuang I L 2008 *Phys. Rev. Lett.* **101** 180602

[35] Wang S X, Ge Y, Labaziewicz J, Dauler E, Berggren K and Chuang I L 2010 *Appl. Phys. Lett.* **97** 244102

[36] Sedlacek J A, Stuart J, Slichter D H, Bruzewicz C D, McConnell R, Sage J M and Chiaverini J 2018 *Phys. Rev. A.* **98** 063430

[37] Zeng J, Yan X T, Yao Y, Zhao Y J, Chen L and Feng M 2023 *Phys. Rev. A.* **108** 023121

[38] Daniilidis N, Gerber S, Bolloten G, Ramm M, Ransford A, Ulin-Avila E, Talukdar I and Häffner H 2014 *Phys. Rev. B.* **89** 245435

[39] An D, Matthiesen C, Urban E and Häffner H 2019 *Phys. Rev. A.* **100** 063405

[40] de Leon N P, Itoh K M, Kim D, Mehta K K, Northup T E, Paik H, Palmer B S, Samarth N, Sangtawesin S and Steuerman D W 2021 *Science* **372** 6539

[41] Lordi V and Nichol J M 2021 *MRS Bull.* **46** 589

[42] Brown K R, Chiaverini J, Sage J M and Häffner H 2021 *Nat Rev Mater.* **6** 892